Size evolution of electronic properties in free antimony nanoclusters

S. Urpelainen,[1,2,*] M. Tchaplyguine,[2] M.-H. Mikkelä,[1] K. Kooser,[3] T. Andersson,[4] C. Zhang,[4] E. Kukk,[3] O. Björneholm,[4] and M. Huttula[1]

[1]*Department of Physics, University of Oulu, P.O. Box 3000, 90014 Oulu, Finland*
[2]*MAX IV Laboratory, Lund University, P.O. Box 118, SE-221 00 Lund, Sweden*
[3]*Department of Physics and Astronomy, University of Turku, 20014 Turku, Finland*
[4]*Department of Physics and Astronomy, Uppsala University, P.O. Box 516, 75120 Uppsala, Sweden*

(Received 12 January 2012; revised manuscript received 19 November 2012; published 10 January 2013)

The evolution of electronic properties in free antimony (Sb) nanoclusters as a function of the cluster size has been studied experimentally using synchrotron radiation. Antimony 4*d* core-level and valence-band regions have been probed, and the 4*d* binding energies and valence ionization potentials of clusters of various mean sizes have been determined. The binding-energy shifts with respect to polycrystalline solid have been used for deriving the electronic properties of the clusters. The observed results suggest that even large Sb clusters are not metallic.

DOI: 10.1103/PhysRevB.87.035411 PACS number(s): 36.40.Mr, 36.40.Cg, 36.40.Ei

I. INTRODUCTION

Recently a new electronic phase of matter promising a novel class of materials for quantum computing and spintronics applications has been discovered. These novel materials, called topological insulators, are insulating in the bulk but contain conducting surface states—so-called topological surface states (TSS). The TSS can give rise to such unique phenomena as the topological magnetoelectric effect, the superconducting proximity effect, and the possibility of hosting magnetic monopoles and Majorana fermions.[1,2] The origin of the TSS has been realized to lie in the spin-orbit interaction. Indeed, they are found in compounds containing heavy elements such as semimetals Bi and Sb. Especially interesting is the case of pure Sb (111) surfaces, which have been recently shown to contain TSS.[3] The problem with the solid-state materials, however, is that they are not actually insulating at room temperature and that only a small fraction of the atoms are located on the surface. The TSS compete with the bulk states, and this has directed the search for materials with TSS toward thin films, nanoribbons, and nanowires.[2,4]

Nanoclusters consisting of a few to several thousands of atoms have a large fraction of their constituents on the surface. For instance, clusters having a geometry close to that of a sphere consisting of 100 and 100 000 atoms (a radius of approximately 1–20 nm) have more than 85 and 10% of the atoms on their surfaces, respectively. In addition, the search for TSS in clusters is motivated by the fact that small clusters are known to have very different electronic properties compared with their solid-state counterparts, and, moreover, these properties vary as a function of cluster size.[5,6] Thus, nanoclusters can be also considered as a solution for the problems associated with the bulk states in topological insulators. Metal clusters are especially promising in this regard, as in many cases they turn into insulators, when they become sufficiently small (see, e.g., Refs. 7–11). In this work, we have studied the size dependent evolution of electronic properties in Sb nanoclusters using synchrotron-radiation excited photoelectron spectroscopy. In the chosen photon energy range, this method is surface sensitive and thus suits optimal probing of the electronic properties of the cluster surfaces.

Small antimony clusters consisting of up to 36 atoms (a characteristic dimension or radius $R < 1$ nm) have been suggested to be nonmetallic[12] by comparing the experimentally derived ionization potentials (IP) with the values obtained from the classical conducting sphere approximation (CSA).[13] In this approximation, the cluster IP dependence on the reciprocal of the cluster radius (R) is a line with a slope practically independent of the parent material. In the limit $R \to \infty$, the line crosses the ordinate axis at the IP of the corresponding solid material, i.e., the work function. The experimental IP values presented in Ref. 12 differ from the CSA prediction by up to more than 2 eV. In the present work, clusters in a wide size range have been created: from the sizes studied in Ref. 12 up to clusters with R of approximately several nanometers. Two separate cluster sources have been employed to cover such a wide size range. The smaller clusters have been produced using the so-called exchange metal cluster source (EXMEC),[14] and the larger ones have been produced using a gas aggregation cluster source (GAS).[15] In the present work, we have obtained both the IPs of the valence electronic shells of Sb clusters and their 4*d* core-level binding-energy values. The obtained results suggest that the properties of Sb clusters up to relatively large (several nanometers) sizes differ considerably from those of solid Sb showing no signs of metallic behavior.

II. EXPERIMENTS

The experiments were carried out at the beam line I411 at MAX-lab (Lund, Sweden).[16] In both experiments (with the EXMEC and GAS cluster sources), Ar was involved as carrier gas and its 3*s* photosatellite lines were used for energy calibration of the 4*d* spectra. The valence spectra were energy calibrated using the well-known energies of Sb_4 valence photoelectrons in the case of EXMEC and the Ar 3*p* photo lines in the case of GAS.

In the studies of smaller clusters (EXMEC), a preformed beam of Ar clusters is let through a resistively heated oven, where it interacts with the Sb_4 clusters (solid Sb evaporates predominantly as Sb_4 tetrahedra[17]). The latter condense on the Ar clusters and are carried further to the interaction region. Gradually, the weakly bound Ar atoms are—partially or completely—evaporated off the Ar_nSb_m complexes in the

heat exchange process. This means that in this work some of the Sb clusters might be adsorbed on or embedded in Ar clusters. However, the interaction between the Ar cluster and the Sb cluster adsorbed on it can be neglected due to the inert nature of Ar clusters, i.e., the weak Van der Waals bonding between the Sb and Ar atoms.

The mean size of the Sb clusters was controlled by changing the collision region sample density, i.e., varying the temperature of the oven in the range 660–725 K. For producing the larger clusters (GAS source), the Sb sample was evaporated from a resistively heated crucible into a flowing liquid-nitrogen-cooled Ar atmosphere (1–2 mbars), where the cluster growth occurred. The core-level 4*d* photoelectron spectra (PES) were recorded at a photon energy of 90 eV. The valence PES were recorded at photon energies of 50 and 60.5 eV with the EXMEC and GAS, respectively. The spectra were recorded at several fixed oven temperatures in the EXMEC source (*a*–*e*) and at one set of conditions for the GAS source (*f*).

In the experiments with the EXMEC source, the emitted electrons were detected using a Scienta R4000 electron energy analyzer. The electrons were detected at 90° with respect to the electric-field vector of the linearly polarized radiation. In the experiments with GAS, the electrons were detected using a modified Scienta SES-100 electron energy analyzer[18] at 0° with respect to the electric-field vector of the linearly polarized radiation. As opposed to the EXMEC source, a complete condensation of Sb_4 into large clusters was observed in GAS, and therefore the spectra recorded using GAS lack the signal from Sb_4.

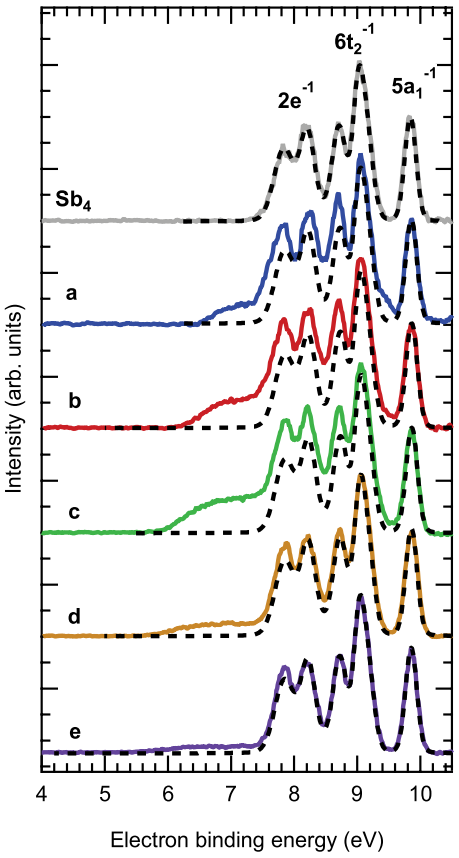

FIG. 1. (Color online) The recorded valence PES using the EXMEC source together with the pure Sb_4 spectrum. The dashed lines show the least-squares fit to the pure Sb_4 signal, which was subtracted away from the spectra. The spectra have been normalized to the $5a_1^{-1}$ signal of Sb_4.

III. RESULTS AND DISCUSSION

A. Valence-band PES

The valence PES recorded using the EXMEC source are presented in Fig. 1 together with the Sb_4 valence PES. As the signal of the parent Sb_4 clusters is always present (in the case of the EXMEC source) and overlaps with that of the larger clusters, a least-squares fit was generated for the well-known pure Sb_4 signal,[19] and the fit was then subtracted from the valence PES recorded at the cluster producing conditions. The valence region PES of Fig. 1 with the Sb_4 signal subtracted are presented in Fig. 2. In the present study, at each set of conditions clusters with a certain size distribution were created, and as a result the valence region photoelectron spectrum is a superposition of signals from all the sizes present in the distribution. For a definite size of clusters, the binding-energy onset of its valence PES reflects the cluster's IP. The onset of the superposition of the valence bands of the whole ensemble of clusters reflects, then, the IP of the clusters *larger* than the mean size produced (that have a lower IP), but the information on the most abundant clusters in the distribution is not readily extractable. Furthermore, the obtained valence PES show complex discrete structures arising from smaller cluster sizes. Thus, determining the IP of clusters from the valence PES containing signals from various cluster sizes is not straightforward and is prone to error. Therefore, one has to work with *averages*, and the following discussion is presented for the *estimated mean size* of the clusters. Typically, for estimating the size of metal clusters, the CSA is used. However, the large deviations of experimental valence IPs from the CSA obtained for size selected clusters by Rayane *et al.*[12] show that the CSA method cannot be implemented—at least for the smaller clusters—using the valence IPs.

Spectrum *a* of Fig. 2 shows three distinct discrete features at peak energies of 7.6, 8.5, and 9.5 eV together with a bandlike structure with its onset at approximately 6.5 eV. These features cannot originate from the Sb_4 clusters, as their signal has been already subtracted from the spectrum. Rayane *et al.*[12] have reported IPs in the range from 7.6 eV down to 7.12 eV for clusters in the size range $N = 9$–37 (R would be approximately in the range 0.4–0.7 nm). The most intense peak at 7.6 eV and the bandlike structure are well within this energy range, indicating that the cluster beam contains clusters with their size distribution somewhere in the above-mentioned region. As the binding energies of the two remaining discrete features are higher than any IP observed by Rayane *et al.*, the two features cannot be the first ionized states of clusters in this size range and thus could originate from the inner molecular orbitals or from various splitting effects such as spin-orbit interaction in the smaller clusters in the beam. The weighted average of the ionization potential for the bandlike structure and the first intense discrete structure is 7.2 eV, giving the *mean IP* of the clusters. This corresponds to a mean size of $\langle N \rangle \approx 30$ (or $\langle R \rangle \approx 0.6$ nm) according to the data by Rayane *et al.* This

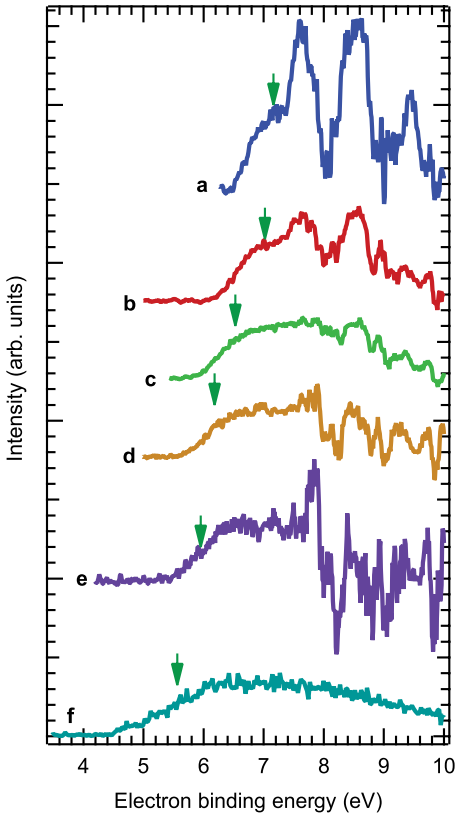

FIG. 2. (Color online) The EXMEC valence PES with the least-squares fits of the Sb_4 signal subtracted away (a–e) together with the valence PES recorded with the GAS (f). The spectra have been normalized to the bandlike structure at around 7.0 eV. The green arrows show the position of the weighted average corresponding to the IP of the mean cluster size.

observation gives a basis for our cluster size estimation in the following discussion.

In spectrum b (Fig. 2), the bandlike structure is enhanced with respect to the three discrete structures at the higher binding energies. In spectra c to f, the band structure becomes broader, and the onset of this valence band shifts toward smaller energies as the cluster size increases. This is expected, as the density of states in the valence band should increase with increasing cluster size, approaching the width of the solid Sb valence band as the coordination of the atoms increases. The weighted averages of the valence-band IPs for spectra a to f calculated in the range from the band onset to the top of the band are presented in Table I.

B. 4*d* core PES

The recorded 4d PES are presented in Fig. 3. The spectra are recorded at the same experimental conditions as the corresponding valence PES. The core-level photo lines from clusters of a definite size have practically symmetric Voigt-like profiles, in spite of the fact that in the present work the observed 4d photoelectron spectrum in each case is a superposition of photo lines from the entire ensemble of nanoclusters (as well as from Sb_4 when using EXMEC). The well-resolved $4d_{5/2}$ component (the peaks below 38 eV in Fig. 3) is broadened due to the size dependent binding-energy shifts,[20]

TABLE I. The IPs and $4d_{5/2}$ binding energies of the clusters together with their shifts with respect to the solid Sb using the work function of $W = 4.55$ eV and $E_{5/2} = 36.55$ (the surface component of polycrystalline solid Sb from Ref. 24).

	IP (eV)	$BE_{5/2}$ (eV)	ΔIP (eV)	$\Delta E_{5/2}$	Γ (meV)	$\langle R \rangle$ (nm)
a	7.16	37.76	2.61	1.21	680	0.6[a]
b	7.02	37.53	2.47	0.98	670	0.7[b]
c	6.53	37.40	1.98	0.85	590	0.8[b]
d	6.18	37.17	1.63	0.62	530	1.2[b]
e	5.95	37.10	1.40	0.55	540	1.3[b]
f	5.56	36.71	1.01	0.16	450	4.5[b]

[a]From a comparison with IPs by Rayane *et al.*[12]
[b]Using the $1/R$ fit for 4d ionization.

and the peak maxima in each case correspond to the binding energy of the clusters at the size distribution maximum if a close-to-Gaussian size distribution is assumed. Therefore, we take the maximum of the peak to present the binding energy of the *mean size* of the clusters. It can be clearly seen from spectra a–f of Fig. 3 that the binding energy of the 4d photo lines decreases as the target density, and correspondingly the size of the clusters, increases. This is to be expected, as the

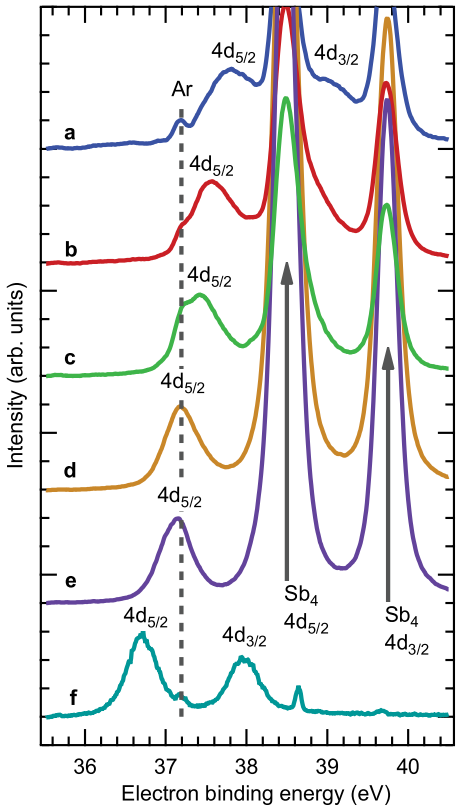

FIG. 3. (Color online) The Sb 4d spectra of Sb clusters. The spectra from a to e have been recorded using the EXMEC source with increasing temperatures. The spectrum f has been recorded using the GAS. All the spectra are normalized to the $4d_{5/2}$ photoelectron line from the clusters. The dashed line shows the position of the Ar 3s satellite line used in energy calibration. The intense spectral lines (exceeding the top of the scale) are the 4d photo lines from the Sb_4 clusters.

coordination number of the atoms in the cluster as well as the screening properties change as the cluster size increases.[21] The $4d_{3/2}$ spectral response from the cluster beam can be resolved from the corresponding Sb_4 response in spectra *a* and *f*. In the other spectra, these two spectral features overlap. The spin-orbit splitting derived from spectra *a* and *f* agrees well with the value of 1.26 eV obtained earlier for the Sb_4 clusters.[22]

To obtain the binding energies, a least-squares fitting assuming the Voigt profiles for all spectral features was performed using the SPANCF curve-fitting procedures for Igor Pro.[23] The $4d_{5/2}$ binding energies of the clusters are presented in Table I together with their full width at half-maximum (FWHM, Γ). It is worth noting that Γ of the clusters $4d_{5/2}$ feature (resolved in all spectra) decreases with the mean cluster size increase, reaching a value of 450 meV in spectrum *f*. The spectra presented by Aksela *et al.*[24] indicate that the width of the 4*d* photo lines for polycrystalline solid Sb is slightly more than 600 meV, and they have been fitted with two peaks 250-meV apart and assigned to the separate responses from the bulk and surface atoms.

In the present work, the larger values of Γ in spectra *a* and *b* can be explained by the size distribution of the clusters[20]—just as the valence-band photoelectron spectrum becomes an overlap of discrete and bandlike structures as the cluster size decreases, so does the 4*d* PES. As the size of the clusters increases from *a* to *f* (Figs. 1–3)—as inferred from the lower $4d_{5/2}$ binding energy and valence IP—so should the bulk-to-surface ratio. If the observed 4*d* spectral features were composed of bulk and surface subcomponents separated by 250 meV, this would make the 4*d* spectral feature broader. In the experiment, in contrast, these features clearly become narrower toward the larger cluster sizes, and no indications of a double peak structure are visible. We infer that even the largest clusters in the present experiments have a relatively large surface-to-bulk ratio.

C. Cluster mean size estimation

By relating our valence spectra and IPs derived from them to the values reported by Rayane *et al.*,[12] we can get a certain estimate of the cluster size for each set of conditions. As Rayane *et al.* pointed out, the experimentally obtained valence IPs deviate significantly from the values calculated (for the dimensions in question) using the CSA approach. For the corresponding 4*d* core-level energies of the clusters, the deviation or the shift from the calculated values appears to be significantly smaller. The shift was calculated with respect to the surface component of the polycrystalline solid motivated by the lack of any indication of a separate bulk response in the present 4*d* PES for clusters. The results should be compared with the CSA-based linear dependence of the binding energy on $1/R$ with the same slope as for the valence IP, but approaching 36.55 eV as $R \rightarrow \infty$. Such a comparison is presented in Fig. 4. Indeed, while the CSA gives valence ionization energies up to 2 eV, too low with respect to the experimental ones (Rayane *et al.*[12]), the core-level binding energies estimated using the CSA differ from the experimental ones by up to only 0.4 eV for Sb_2.

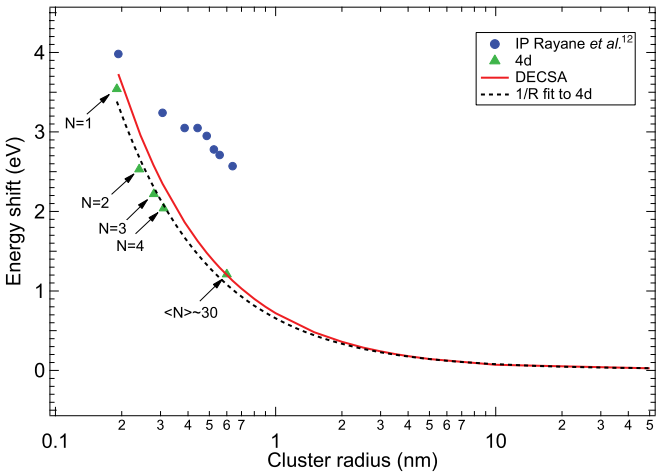

FIG. 4. (Color online) Comparison of the CSA model (solid line) with experimental energy shifts obtained for the IPs (solid circles) of the clusters with respect to the solid work function ($W = 4.55$ eV) and the shifts obtained for the $4d_{5/2}$ binding energies (solid triangles) with respect to the solid surface component for *known* cluster sizes (from Ref. 24 and a comparison of present data with Ref. 12) up to $R \approx 0.6$ nm.

As mentioned above, for the smallest clusters in the present work, the mean size can be estimated by comparing the mean IP of the clusters to the ones obtained by Rayane *et al.*[12] This comparison gives a mean size of $\langle R \rangle = 0.6$ nm of the clusters. The $4d_{5/2}$ binding-energy shift from spectrum *a* gives a value of 1.2 eV with respect to the polycrystalline solid surface value (36.55 eV[24]) and is nearly the same as that obtained from the CSA for clusters with $R = 0.6$ nm.

Core-level energies have been used successfully for estimating the most abundant cluster size in a beam in similar experiments (see, e.g., Ref. 25), but their advantages over the valence response, especially in the small-size range, have not been sufficiently discussed: As mentioned above, the distribution of sizes in the cluster beams causes the onset of the valence band to be a rather poor estimate of the ionization potential of the clusters, as it is the superposition of the valence-band responses from all cluster sizes, whereas the 4*d* features show a simple Voigt spectral profile convoluted with a Gaussian profile emerging from the size distribution. In such a case, the peak position will give the mean binding energy of the clusters. In addition, each cluster in the beam has a size and geometry specific density of states in the valence band, which is further complicated in the photoionization process by the photon energy dependent cross section,[26] which is reflected in the PES. This makes the core-level binding energies far more reliable for the mean size estimation, when a distribution of sizes is present in the cluster beam.

On the other hand, as the screening of the core-hole becomes stronger, evolving from dielectric polarization screening to complete metallic screening, with increasing cluster size,[10] the difference between the CSA prediction and the actual binding-energy shifts becomes increasingly smaller and the size estimate from the CSA becomes more justified. From Fig. 4, it is seen that the difference between the 4*d* binding-energy shift predicted by the CSA and the actual shift of the 4*d* binding energies is small. In addition, the measured

TABLE II. The estimated sizes for the smallest and largest clusters in the beam together with the broadening pertaining to the size distribution Γ_c obtained through deconvolution.

	Γ_c (meV)	$R_{\min}$ (nm)	$\langle R\rangle$[b] (nm)	$R_{\max}$ (nm)
a	500	0.5[a]/0.5[e]	0.6	0.7[c]/0.7[d]
b	490	0.5[a]/0.6[e]	0.7	0.9[c]/0.8[d]
c	400	0.6[a]/0.6[e]	0.8	1.0[c]/0.9[d]
d	340	0.8[a]/1.0[e]	1.2	1.5[c]/1.4[d]
e	350	0.9[a]/1.0[e]	1.3	1.8[c]/1.5[d]
f	280	2.3[a]/3.6[e]	4.5	120[c]/5.2[d]

[a]Using the $1/R$ fit for $E_b + \Gamma_c/2$.
[b]Using the $1/R$ fit except for spectrum *a*, where a comparison with Rayane *et al.*[12] was used.
[c]Using the $1/R$ fit for $E_b - \Gamma_c/2$.
[d]Using $R_{\max} \approx 1.15\langle R\rangle$.
[e]Using $R_{\min} \approx 0.8\langle R\rangle$.

$4d$ binding-energy shifts seem to follow a curve very similar to the one predicted by CSA proportional to $1/R$. Thus, we fit a curve with $1/R$ dependence to the $4d$ binding-energy shifts of known size and use the result in approximating the mean size of the clusters using their $4d$ binding-energy shifts in the spectra from *b* to *f*. The estimated mean sizes of the clusters are presented in Table I.

In addition, we present a rough estimation of the largest and smallest sizes of clusters in the beam by taking a deconvolution of the obtained $4d_{5/2}$ FWHM linewidth with the experimental broadening due to the electron analyzer and photon beam as well as the lifetime broadening of the core-hole state. The remaining energy broadening Γ_c can then be considered to arise mostly from the size distribution of the clusters. Thus, the binding energies $E_b - \Gamma_c/2$ and $E_b + \Gamma_c/2$ can be used to estimate the size of the largest and smallest clusters in the beam, respectively. These approximate size estimations together with the obtained Γ_c are presented in Table II. The results for this estimation seem reasonable, but the $R_{\max}$ obtained for the clusters produced using GAS is obviously too large. This is due to the sensitivity of the CSA approximation at very small energy shifts, where a small difference in the value of the shift can result in a significant change in the radius. Then the order of the magnitude of the error in the determined cluster radius is given by

$$\Delta R\,(\text{nm}) \approx \frac{1\,(\text{eV})}{E_{\text{shift}}^2}\Delta E_{\text{shift}}, \tag{1}$$

where all the energies are given in eV. This means that, for instance, for energy shifts (from the solid value) on the order of 0.01 eV the accuracy of the energy determination should be better than 0.1 meV if the radius is to be determined with an accuracy better than 1 nm. This kind of accuracy is not reached for these experiments. The accuracy of the binding-energy determinations is estimated to be around 50 meV for the EXMEC experiments and 40 meV for the GAS experiments. This gives an error of approximately 100 nm for the determined $R_{\max}$ in the case of GAS, so the estimation for this particular value is not used in the remaining discussion.

For the other estimation of $\langle R\rangle$, $R_{\min}$ and $R_{\max}$, however, the errors (excluding any possible systematic errors) are all below 1.6 nm, making the results plausible. On the other hand, valence-band spectrum *f* (Fig. 2) shows that the onset of the band structure appears at approximately 4.7 eV, which is only 150 meV higher than the solid work function. This indicates that larger clusters (than $\langle R\rangle \approx 4.5$ nm), which have evolved to metallic properties, must also be present in the beam produced with the GAS.

The FWHM of the size distribution of clusters can be typically approximated as $\Gamma_N = \langle N\rangle/2$, where N is the number of atoms in the cluster. When this is converted to the cluster radius—assuming, for simplicity, a spherical cluster geometry—it yields roughly $R_{\max} \approx 1.15\langle R\rangle$. Similarly, the smallest cluster can be estimated as $R_{\min} \approx 0.8\langle R\rangle$. The estimates for the largest and smallest clusters in the beam using this method have also been presented in Table II. This seems to hold very nearly for the size approximations for the EXMEC case. Using this approximation for the case of GAS, the largest size in the distribution would be approximately $R_{\max} = 5.2$ nm, which is quite far from the radius obtained using the FWHM of the $4d_{5/2}$ line in the PES but on the other hand a much more plausible value, due to the large possibility of errors in the maximum size estimation in the case of very small energy shifts, as discussed above. Therefore, we will use the smaller value $R_{\max} = 5.2$ nm in the following discussion as the maximum size in the GAS cluster beam. For the EXMEC case, we use the $R_{\max}$ values obtained using the FWHM of the $4d_{5/2}$ lines in the PES.

D. Discussion

The IP of the clusters as a function of the estimated cluster size is presented in Fig. 5 for $\langle R\rangle$ and $R_{\max}$ together with the size selected data of Rayane *et al.*[12] The IP for the mean size is determined as the centroid of the valence band, and the IP for $R_{\max}$ is determined as the onset of the band, as explained above. As the $1/R$ fit for the $4d$ energy shifts has been used to estimate the sizes of the clusters, the dashed curve in Fig. 5 reflects also the energy shift of the core levels as a function of the cluster size, and the $4d$ data have not been plotted separately.

To explain the large deviations in the valence IPs, Rayane *et al.*[12] have considered the preferred tetrahedral packing of small Sb clusters caused by the strong *sp* hybridization in Sb as a reason for this behavior: The Sb_4 clusters agglomerate into clusters of tetramers and prefer tetrahedral packing,[27] while usually a spherical geometry is assumed when estimating the size of the clusters using the CSA. Whereas most metals evaporate as single atoms and tend to form clusters with geometry close to spherical, and follow relatively well the size dependence of IPs predicted by the CSA, Sb cluster tetrahedral structure creates geometries far from spherical, and the CSA is no longer valid. In the present study, the valence IPs of the smallest mean cluster sizes are in a good agreement with the data obtained by Rayane *et al.*[12]

If we now consider the tetrahedral packing proposed by Sattler *et al.*[17] in context with the present observations, and especially clusters with a pure tetrahedral form, we would expect to see several low-coordination signals in the $4d$ core PES from atoms on edges and corners of the tetrahedron. As no such clear signals are observed in the $4d$ photoelectron

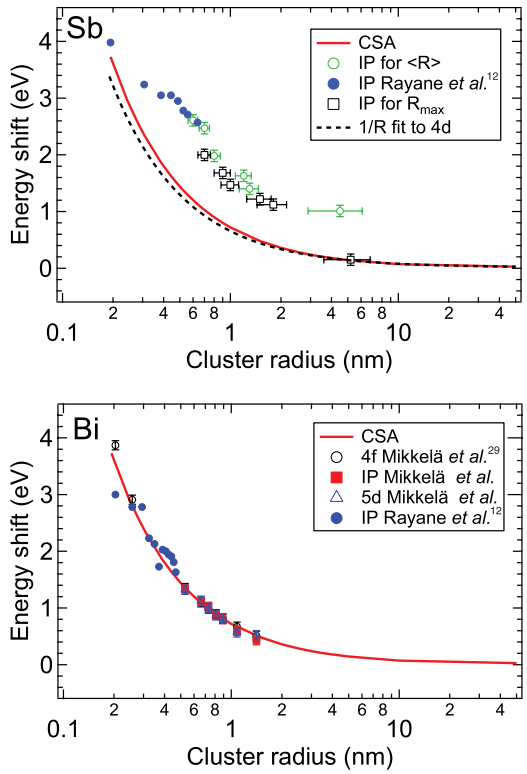

FIG. 5. (Color online) Upper panel: the mean IP shifts for Sb determined in the present work (open circles) together with the ones determined by Rayane *et al.*[12] (solid circles). Lower panel: the various binding-energy shifts for Bi from Ref. 29. The solid line presents the energy shift as a function of cluster size from the CSA. The error bars reflect the error estimates due to inaccuracy in the size estimation, energy calibration, and solid binding energies as well as in determining the valence IP. No possible systematic errors are included.

lines, we infer that the observed clusters must have a smoother, more symmetric structure with no significant amount of low-coordination atoms apart from the cluster surface, especially for the cluster sizes from $\langle R\rangle \approx 0.6$ to ≈ 1.3 nm produced with the EXMEC source. This includes geometries close to spherical but also the possibility of more open inhomogeneous structures lacking long-range order.

After the size of $N = 36$ ($R \approx 0.6$ nm), the IP determined in the present work starts to approach the values obtained from the CSA prediction (Fig. 5) but does not reach it even at sizes with $\langle R\rangle \approx 4.5$ nm. This is, of course, a direct consequence of the fact that the energy shifts from the valence-band ionization potential centroid and the binding energy of the 4*d* core electrons differ from each other, so that the difference becomes smaller and smaller as the cluster size increases. Similar behavior, where the core-level shift is less than the valence shift, has been observed, for instance, in Pd nanoparticles by Aruna *et al.* in the size range 6–20 nm.[28] However, around the size of approximately 4.5 nm the IP shift drops very quickly to the CSA curve, indicating solidlike properties of the clusters. Such a sudden transition is also observed for Hg clusters by Rademann *et al.*[7] albeit at much smaller sizes. In addition, the core 4*d* photo lines do not show any clear asymmetry or higher background due to the Donijah-Sunjic line shape, which would be observable if the clusters were metallic.

This indicates that the valence band and conduction band start to overlap energetically only at nearly macroscopic sizes as opposed to metal clusters of many different materials, where the transition to metallic properties happens typically in the size region from a few tens of atoms to some hundreds of atoms or around $R \approx 1$ nm (see, e.g., Refs. 8–11). This is not surprising, as the extremely narrow overlap of the valence and conduction bands in the solid state makes Sb a poor metal with an indirect negative band gap. At the same time, the observation that even very large Sb clusters are insulating means that the band gap of Sb clusters could be controlled very smoothly above the quantum size regime. One consequence of this is that Sb clusters consisting of a few thousand Sb atoms ($R \approx 3$ nm) could form building blocks for nanoscale electronic devices, as at these sizes the clusters are more easily controlled on substrate surfaces.

Another explanation for the observed behavior is that the clusters have a very open, more amorphous geometry lacking long-range order and clear crystal structure that would be required in order to form a conduction band. Also, this kind of clusters would definitely be insulating.

IV. CONCLUSIONS

In this work, we have presented experimental data on the 4*d* core photoionization and valence photoionization of Sb clusters of various mean sizes. Energy shifts with respect to polycrystalline solid Sb show that the shift for the 4*d* core levels is significantly smaller than the shift for the ionization potentials and that the 4*d* energy shift approaches the CSA already for clusters with a characteristic radius less than 1 nm. The valence ionization potential, on the other hand, differs from the CSA significantly up to sizes estimated to be around 5 nm, indicating a relatively late transition toward the bulk properties of Sb. These results differ significantly from those obtained for Bi clusters in the size range from 0.5 to 1.4 nm,[29] where the core-level shifts are nearly equal to the valence ionization potential shifts already at the smallest sizes and follow the CSA very closely.

Clearly, the peculiar electronic properties of Sb clusters can be traced to their geometry. Indeed, electron-diffraction studies show the Sb clusters to have both crystalline and amorphous structures.[30,31] The crystalline structures observed seem to be faceted structures with a lattice nearly identical to the bulk rhombohedral geometry. The most probable geometries of the clusters in the size regime of a few thousands of atoms are four different kinds of faceted structures, three of which contain one or two {111} surfaces. This indicates that the largest nonconducting clusters observed in this study could both contain {111} surfaces hosting TSS and in the conventional sense be truly insulating.

Moreover, studies on Sb nanocluster island growth on amorphous carbon surfaces show that Sb clusters in this size range maintain their size when deposited on surfaces, whereas smaller clusters move more freely to form larger islands.[32] Thus, the electronic properties are also more likely maintained, given that the interaction between the surface and the cluster

is weak. This could present a possibility of constructing truly insulating topological insulators out of Sb nanoclusters deposited on surfaces.

However, the exact geometry of the clusters remains to be determined. The conjunctions made here could in the future be further verified by embedding the clusters on surfaces and performing angle-resolved photoelectron spectroscopy to map their band structure. Recent developments in advanced electron optics, production quality of x-ray optics and beams in modern synchrotron-radiation facilities, enable the probing of the target in—or focusing the beam down to—the nanometer scale. This should make it possible to study the electronic properties of single clusters in the near future.

ACKNOWLEDGMENTS

This work has been financially supported by the Research Council for Natural Sciences of the Academy of Finland, the Swedish Research Council (VR), the Knut and Alice Wallenberg Foundation (KAW), and the European Community Research Infrastructure Action under the FP6 "Structuring the European Research Area" Program (through the Integrated Infrastructure Initiative "Integrating Activity on Synchrotron and Free Electron Laser Sciences"). S. U. would like to acknowledge Lund's University for financial support. M.-H. M. was financed by the Vilho, Kalle, and Yrjö Väisälä foundation. We thank the staff of MAX-lab for their assistance.

*samuli.urpelainen@maxlab.lu.se

[1] D. Hsieh, D. Qian, L. Wray, Y. Xia, Y. S. Hor, R. J. Cava, and M. Z. Hasan, Nature (London) **452**, 970 (2008).
[2] M. Z. Hasan and C. L. Kane, Rev. Mod. Phys. **82**, 3045 (2010).
[3] J. Seo P. Roushan, H. Beidenkopf, Y. S. Hor, R. J. Cava, and A. Yazdani, Nature (London) **466**, 343 (2010).
[4] H. Peng, K. Lai, D. Kong, S. Meister, Y. Chen, X.-L. Qi, S.-C. Zhang, Z.-X. Shen, and Y. Cui, Nature Mater. **9**, 225 (2010).
[5] W. A. de Heer, Rev. Mod. Phys. **65**, 611 (1993).
[6] B. von Issendorff and O. Cheshnovsky, Annu. Rev. Phys. Chem. **56**, 549 (2005).
[7] K. Rademann, B. Kaiser, U. Even, and F. Hensel, Phys. Rev. Lett. **59**, 2319 (1987).
[8] O. Cheshnovsky, K. J. Taylor, J. Conceicao, and R. E. Smalley, Phys. Rev. Lett. **64**, 1785 (1990).
[9] R. Busani, M. Folkers, and O. Cheshnovsky, Phys. Rev. Lett. **81**, 3836 (1998).
[10] V. Senz *et al.*, Phys. Rev. Lett. **102**, 138303 (2009).
[11] J. Bowlan, A. Liang, and W. A. de Heer, Phys. Rev. Lett. **106**, 043401 (2011).
[12] D. Rayane, P. Melinon, B. Tribollet, B. Cabaud, A. Hoareau, and M. Broyer, J. Chem. Phys. **91**, 3100 (1989).
[13] G. Makov, and A. Nitzan, J. Chem. Phys. **88**, 5076 (1988).
[14] M. Huttula, M.-H. Mikkelä, M. Tchaplyguine, and O. Björneholm, J. Electron Spectrosc. Relat. Phenom. **181**, 145 (2010).
[15] E. Kukk *et al.* (private communication).
[16] M. Bässler *et al.*, Nucl. Instrum. Methods A **469**, 382 (2001).
[17] K. Sattler, J. Mühlbach, and E. Recknagel, Phys. Rev. Lett. **45**, 821 (1980).
[18] M. Huttula, M. Harkoma, E. Nõmmiste, and S. Aksela, Nucl. Instrum. Methods Phys. Res. A **467**, 1514 (2001).
[19] S. Urpelainen, A. Caló, L. Partanen, M. Huttula, J. Niskanen, E. Kukk, S. Aksela, and H. Aksela, Phys. Rev. A **80**, 043201 (2009).
[20] G. K. Wertheim, Z. Phys. B **66**, 53 (1987).
[21] W. F. Egelhoff, Jr., Surf. Sci. Rep. **6**, 253 (1987).
[22] S. Urpelainen, A. Caló, L. Partanen, M. Huttula, S. Aksela, H. Aksela, S. Granroth, and E. Kukk, Phys. Rev. A **79**, 023201 (2009).
[23] E. Kukk, computer code SPANCF, http://www.physics.utu.fi/en/department/materials_research/materials_science/Fitting.html.
[24] S. Aksela, M. Patanen, S. Urpelainen, and H. Aksela, New. J. Phys. **12**, 063003 (2010).
[25] M. Tchaplyguine *et al.*, J. Electron Spectrosc. Relat. Phenom. **166-167**, 38 (2008).
[26] K. Jänkälä, M. Tchaplyguine, M.-H. Mikkelä, and O. Björneholm, and M. Huttula, Phys. Rev. Lett. **107**, 183401 (2011).
[27] K. Sattler, J. Mühlbach, P. Pfau, and E. Recknagel, Phys. Lett. A **87**, 418 (1982).
[28] I. Aruna, B. R. Mehta, L. K. Malhortra, and S. M. Shivaprasad, J. Appl. Phys. **104**, 064308 (2008).
[29] M.-H. Mikkelä, M. Tchaplyguine, S. Urpelainen, K. Jänkälä, O. Björneholm, and M. Huttula, J. Appl. Phys. **112**, 084326 (2012).
[30] M. Kaufmann, A. Watt, J. G. Partridge, S. A. Brown, Eur. Phys. J. D **34**, 29 (2005).
[31] M. Kaufmann, Ph.D. thesis, University of Canterbury, 2006.
[32] B. Yoon, V. M. Akulin, Ph. Cahuzac, F. Carlier, M. de Frutos, A. Masson, C. Mory, C. Colliex, and C. Bréchignac, Surf. Sci. **443**, 76 (1999).